J Supercond Nov Magn (2014) 27:1403–1412
DOI 10.1007/s10948-014-2477-4

ORIGINAL PAPER

Improvement of the Nature of Indentation Size Effect of Bi-2212 Superconducting Matrix by Doped Nd Inclusion and Theoretical Modeling of New Matrix

O. Ozturk · E. Asikuzun · S. Kaya · G. Yildirim · M.B. Turkoz · A. Kilic

Received: 27 December 2013 / Accepted: 2 January 2014 / Published online: 25 January 2014

Abstract Neodmium (Nd) inclusions at different stoichiometric ratios ($x = 0.0$, 0.001 %, 0.005 %, 0.01 %, 0.05 %, 0.1 %) are doped in the Bi-2212 superconducting samples and the samples obtained are subjected to the sintering process at 840 °C constant temperature for 72 hours. The effect of Nd doping on the structural and mechanical properties of prepared samples is investigated by the standard characterization measurements. XRD and SEM measurements are performed to obtain information about surface morphology, phase ratios, lattice parameters and particle size. Moreover, Vickers microhardness (H_V) measurements are exerted to investigate the mechanical properties of the all samples in detail. It is found that all the properties given above retrogress with the increase of the Nd concentration in the Bi-2212 superconducting core. However, the ISE nature of the materials improves systematically. Additionally, the experimental results of microhardness measurements are analyzed using Meyer's law, PSR, MPSR, EPD models and HK approach. The results show that Hays–Kendall approach is determined as the most successful model.

O. Ozturk · E. Asikuzun (✉) · S. Kaya
Department of Physics, Kastamonu University, 37100 Kastamonu, Turkey
e-mail: easikuzun@kastamonu.edu.tr

G. Yildirim
Department of Mechanical Engineering, Abant Izzet Baysal University, 14280 Bolu, Turkey

M.B. Turkoz
Department of Physics, Kırıkkale University, 71450 Kırıkkale, Turkey

A. Kilic
Department of Physics, Ankara University, 06100 Ankara, Turkey

Keywords XRD · SEM · Meyer's law · HK approach · ISE

1 Introduction

The hardness of a material is one of the important mechanical properties such as elasticity, ductility and toughness. Hardness can be defined as the resistance to a hard object that is sunk on the specimen surface and determined using the size of permanent or plastic indentation created on the surface in certain conditions. There are various hardness measurement methods, such as Vickers, Brinell, Rockwell, Knopp and Berkovich models, developed with regard to the shape of used indenter tip, the applied load and the indentation size. The theoretical results obtained at the same conditions should be compared each with the others to find more appropriate results with the experimental evidences [1].

In recent years, one of the reasons of the increase in researches related to the indentation tests has been the interpretation of the role of plastic deformation at the initial stages of plastic deformation. Another reason is to investigate the interpretations of great hardness values under small applied loads. On the other hand, careful monitoring of the initial stages of plastic deformation under small indentation test loads will help in better understanding of the fundamental nature of the indentation tests. This interest in indentation tests has given a new dimension to the studies until now related to the behavior of the indentation load/deformation and the observation of material structure that has been applied in indentation test [2]. It is well known that microhardness depends sensitively on the applied test load in experiments on different materials [3–8].

Microhardness emerges as Indentation Size Effect (ISE) and Reverse Indentation Size Effect (RISE) behavior. The

former feature decreases with the enhancement of the applied indentation test load whereas the latter one increases with increasing the load applied. For the both cases, the hardness remains unchanged after reaching specific critical load value. The ISE behavior is also based on characteristics such as the elastic recovery of the indentation [9, 10], the composed hardening during the chipping process [11], the required minimum load for the starting of plastic deformation, the size of dislocation loops during the chipping process [12], the response of material to elastic/plastic deformation [13], the relationship of the friction resistance between indenter/sample with the elastic resistance [14, 15], and the chemical pollutions or the oxidation occurring on the surface [16].

In this study, SEM and XRD measurements are performed for the investigation of structural properties of pure and Nd-doped Bi-2212 superconducting samples. Besides, Vickers microhardness test method used for the characterization of the mechanical properties is the main objective of this study. It is found that all the samples exhibit the ISE behavior. In addition, the experimental findings are examined by the available theoretical models proposed in the literature and the results show that Hays–Kendall approach is found to be the most suitable model in defining the microhardness of the samples.

2 Experimental Details

In this study, Nd_2O_3 (99.9 % purity, Alfa Aesar Co., Ltd.) powder is added to Bi-2212 (99.9 % purity, Alfa Aesar Co., Ltd.) superconductor powder in the ratios of $x = 0.0$, 0.001, 0.005, 0.01, 0.05 and 0.1 %. The obtained powders are pressed into tablets of 13 mm in diameter and 1–1.5 mm thick under the constant pressure of 7 tons. Then the tablets are subjected to sintering process at 840 °C for 72 hours with 5 °C/min heating and cooling rates.

The SEM analysis is performed using a JEOL JSM-6390LV model scanning electron microscope when the evaluation of the crystal structure and lattice parameters belonging to the samples studied in this work is carried out by a Bruker D8 Advance model diffractometer with CuK_α radiation ($\lambda = 1.5418$ Å) in the range $2\theta = 5$–$60°$ at a scan speed of 1.2 deg/min and a step increment of 0.08° at room temperature. Moreover, EDS measurements investigate the change in ion quantity with Nd addition in all the samples.

In addition, the mechanical characteristics of undoped and Nd-doped Bi-2212 superconducting ceramics are examined by means of the Vickers microhardness measurements conducted by a digital microhardness tester (Shimadzu HMV-2). The experimental evidences obtained from microhardness measurements have also been analyzed by the presently available theoretical hardness models being proposed in the literature. Based on the results obtained, the models studied have been compared each with the others and the most appropriate model was determined for the Nd-doped Bi-2212 superconducting materials. The superconducting samples with 0.0, 0.001, 0.005, 0.01, 0.05 and 0.1 % will hereafter be denoted as $M0$, $M1$, $M2$, $M3$, $M4$ and $M5$, respectively.

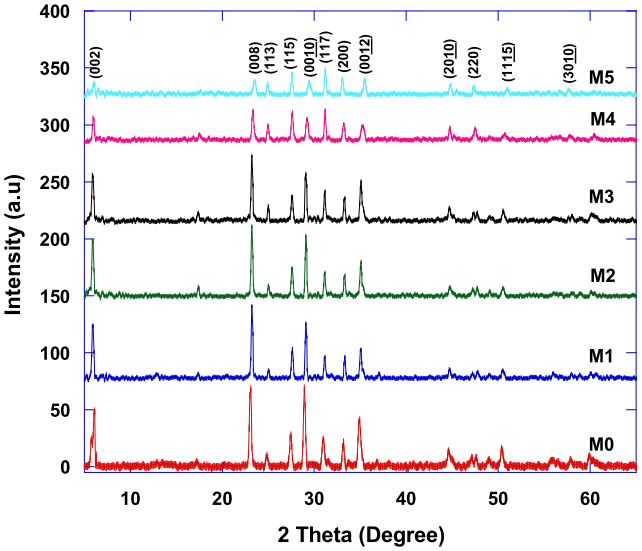

Fig. 1 XRD patterns of all the samples

Table 1 XRD measurement results for the samples

Samples	c (Å)	a (Å)	Volume fracture		Grain size (nm)
			Bi-2212 (%)	Bi-2201 (%)	
M0	31.33	5.35	95	5	107.86
M1	30.49	5.37	96	4	97.29
M2	30.45	5.38	93	7	85.41
M3	30.43	5.39	91	9	61.85
M4	30.26	5.40	86	14	47.38
M5	30.06	5.41	78	22	34.33

3 Results and Discussion

3.1 XRD Analysis

XRD measurements of $M0$, $M1$, $M2$, $M3$, $M4$ and $M5$ samples prepared by solid-state reaction method are conducted in the range of $2\theta = 3 - 60°$ at a scan speed of 3°/min at room temperature. Figure 1 shows the results of XRD measurement patterns for each sample studied [17, 18]. As seen from Table 1, parameter c of the samples decreases from 31.33 to 30.06 Å with increasing Nd doping in the crystal structure as a consequence of the decrement in the

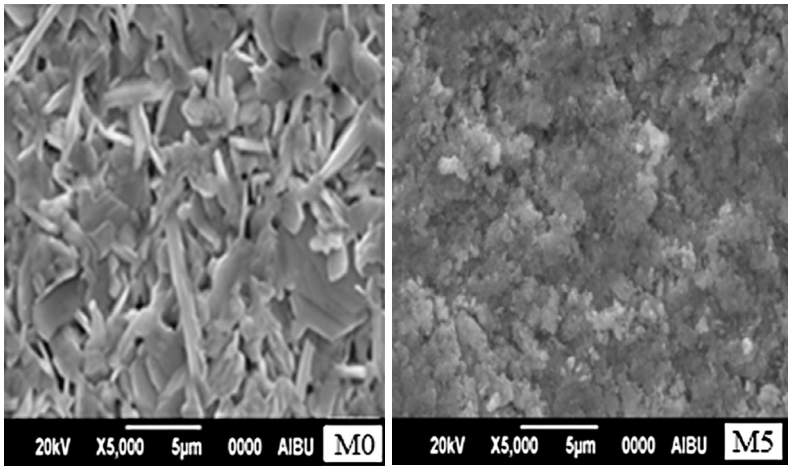

Fig. 2 SEM micrographs of (**a**) M0 and (**b**) M5 samples

net positive charge (valency) in the Bi–O layers [19]. On the other hand, the lattice constant a tends to increase with the increment in the Nd addition level in the system. The fundamental reason of the increment is in the extra electrons in anti-bonding orbital due to the increase of the effective Cu valence. Based on the lattice parameter evidences, it would be more precise to say that the dopant atoms are properly incorporated into the Bi-2212 superconducting core and solved partially [20, 21]. It is another important result obtained from the XRD patterns that the Bi-2212 superconducting phase decreases while the Bi-2201 phase starts to increase with the enhancement of the Nd additives inserted in the superconducting matrix. Regardless, Fig. 1 confirms that the Bi-2212 phase is dominant for all the samples produced.

3.2 Grain Size Calculation by Scherrer–Warren Equation

Grain size value, determined from the X-ray diffraction patterns, is one of the most important characteristics for the engineering, industrial and technological applications of the superconducting materials. This value can be calculated with the well-known Scherrer–Warren method as given by [17, 22]:

$$D = \frac{0.941\lambda}{B\cos\theta_B} \tag{1}$$

$$B^2 = B_m^2 - B_s^2 \tag{2}$$

where D denotes the grain size, λ the wavelength of the X-ray used and B the full width half of the maximum peak intensity in the radian unit. Also, B_m is a constant value and θ is an angle belonging to this peak. The results of the grain size calculations are detailed in Table 1. It is obvious from the table that the grain size value tends to decrease dramatically with the increase of the Nd inclusion in the Bi-2212 superconducting matrix. The largest value of 107.86 nm is calculated for the virgin sample whereas this value reduces to 34.33 nm for the M5 sample. This result is supported by the SEM images.

3.3 SEM Analysis

In this part of the paper, the surface morphology of the samples prepared is studied with the aid of Scanning Electron Microscopy (SEM). That the microstructural properties degrade systematically with the increase of the Nd decorations in the Bi-2212 superconducting core is realized clearly. Thus, we depict only the pure (best) and 0.1 % Nd-doped (worst) sample images. One can see the SEM images (taken in the secondary electron image mode at 5000-X magnification) of undoped and $x = 0.1$ % Nd-doped samples in Fig. 2. It is apparent from the figure that the former sample obtains the smoother and denser morphology with the clear and characteristic flaky slabs of large platelet-like structure [23–27]. Additionally, the degradation of the crystal plane alignment (melting), crystallinity, grain connectivity and layered grain growth confirm that the Nd impurities are unfavorable for the formation of the Bi-2212 superconducting phase due to the deterioration of the superconducting matrix. It is another supposition that the porosity increases with the doping level as a consequence of the decrement in the crystalline sizes, being favored by the results of the XRD examinations.

3.4 Energy Dispersive Spectroscopy (EDS) Analysis

Energy dispersive spectroscopy (abbreviated EDS) is one of the most commonly used methods of detecting the quantitative values of the atomic composition. In the current work, elemental composition analysis of the elements and ions in the undoped and Nd-doped Bi-2212 superconducting samples has been carried out systematically. Similarly to the

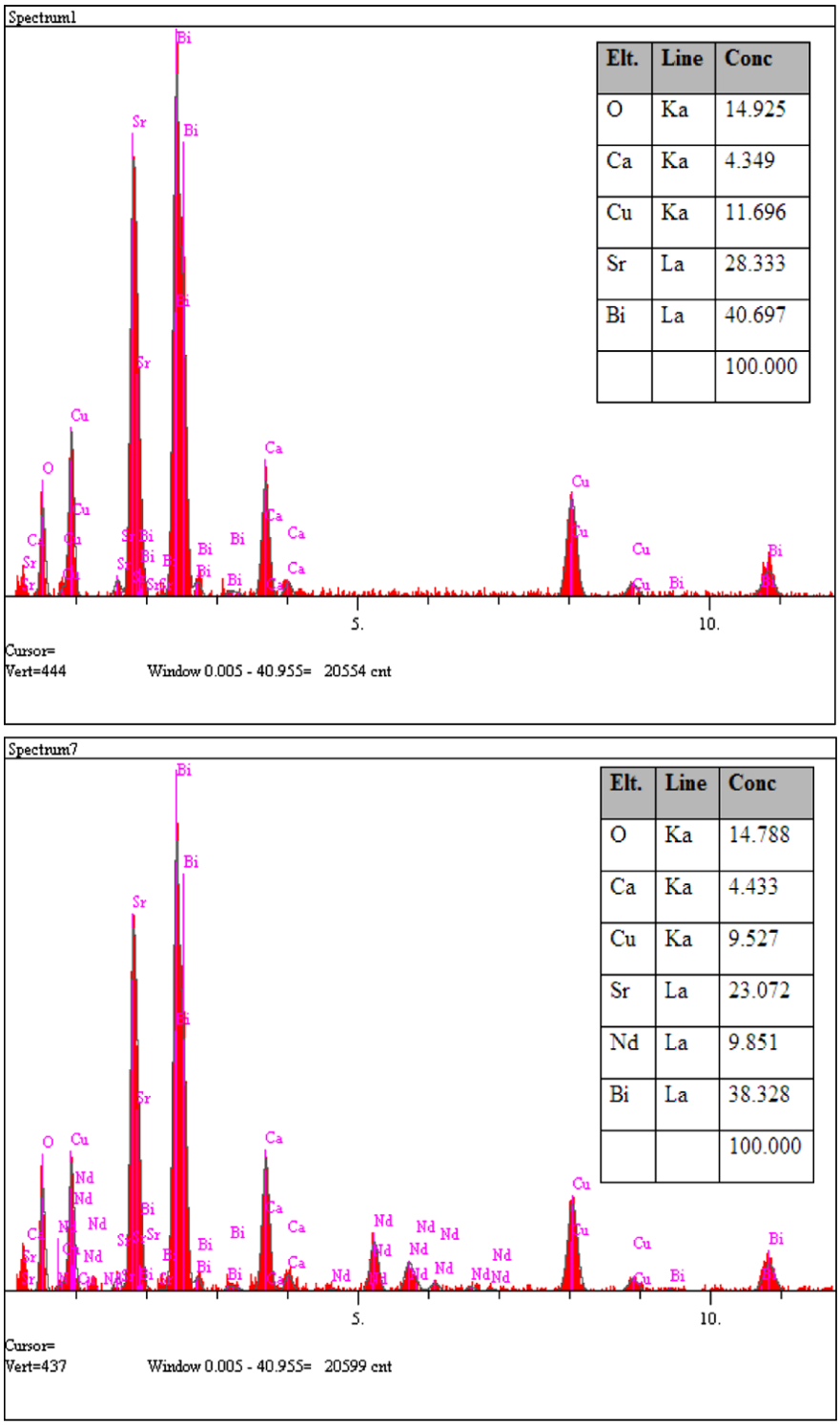

Fig. 3 EDS patterns of (**a**) $M0$ and (**b**) $M5$ samples

SEM analysis part, we here discuss only the EDS spectrum of the $M0$ (best) and $M5$ (worst) samples. One can see from Fig. 3 that there is no difference between the superconducting materials except for the Nd impurity peak (graphical red blocks). This is attributed to the fact that the Nd inclusions in the system are effectively entered into the microstructure of the Bi-2212 superconducting phase. As for the numerical findings in the figure, the amounts of all the elements except oxygen used in the preparation of the Bi-2212 phase tend to change with the Nd doping element in the structure. The Ca element level hardly increases whereas the Cu and Bi elements decrease slightly with the doping. However,

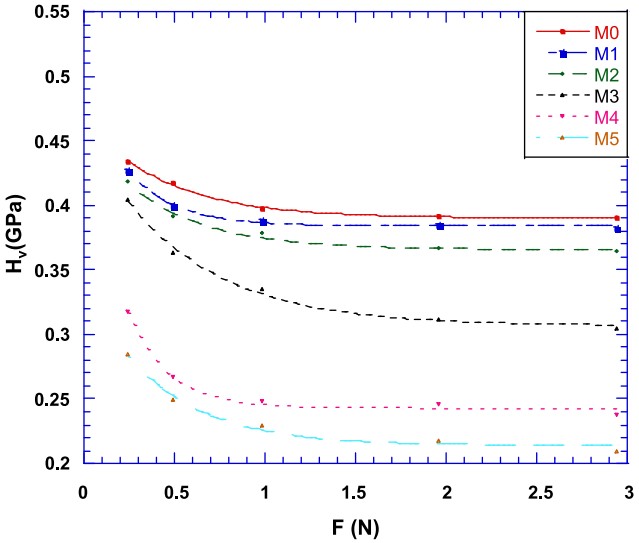

Fig. 4 The variations of microhardness with load for the samples

the decrement in the Sr element is noted dramatically. This might be associated with the fact that the Nd elements incorporate into the crystal structure by replacing Sr elements, verifying that the Nd inserted in the Bi-2212 system causes superconducting properties to deteriorate [28–30].

3.5 Vickers Microhardness Analysis

In this paper, the Vickers microhardness measurements allow us to determine the mechanical properties of the $M0$, $M1$, $M2$, $M3$, $M4$ and $M5$ samples prepared by solid-state reaction method at different proportions ($x = 0.0$, 0.001, 0.005, 0.01, 0.05 and 0.1 %). As is well known, the mechanical characterization of ceramic materials plays an important role in their technological applications and the real (true) microhardness of a material can be calculated from the relation

$$H_V = 1854 \times 4\left(\frac{F}{d^2}\right) \tag{3}$$

One can see in detail the change of the load-dependent microhardness values as a function of the test load in Fig. 4. The microhardness values of each sample decrease with increasing both the Nd doping level and the applied load. The first reason (decrement with the doping) is in the degradation of interaction between superconducting grains [31]. The second reason is in the typical Indentation Size Effect (*ISE*) behavior, and it is not wrong to say that the elastic recovery plays a dominant role in the Bi-2212 superconducting ceramics prepared in this work. Another interesting result is that the reduction of the Vickers microhardness values with the applied load is far more pronounced than that of the values with the Nd doping. Other mechanical properties such as elastic modulus ($E = 81.9635 H_V$), yield strength ($Y \approx \frac{H_V}{3}$) and fracture toughness ($K_{IC} = \sqrt{2E\gamma}$) can theoretically be computed by the real microhardness values. It is to be mentioned here that the mechanical values given above vary from material to material. The variation of the parameters against the applied indentation test loads is numerically tabulated in Table 2. It is visible from the table that the load-dependent values of E, Y and K_{IC} decrease with the increase of both the Nd content and the applied test load. It is also known from the literature that these parameters strongly depend upon the applied load for the ceramics exhibiting the ISE feature [32, 33]. Additionally, several models describe the microhardness characteristics and behavior (ISE or RISE) of the samples [34–36]. In this paper, the Meyer's law, the Hays–Kendall approach (HK), the proportional sample resistance (PSR), the modified proportional sample resistance (MPSR) and the elastic/plastic deforma-

Table 2 The calculated load-dependent H_V, E, Y and K_{IC} for the samples

Samples	F (N)	H_V (GPa)	E (GPa)	Y (GPa)	$K_{IC} \times 10^3$ (Pa/m$^{1/2}$)
M0	0.245	0.434	35.57	0.144	272.13
	0.490	0.417	34.17	0.139	266.75
	0.980	0.397	32.53	0.132	260.28
	1.960	0.392	32.12	0.130	258.63
	2.940	0.390	31.96	0.130	257.97
M1	0.245	0.427	34.99	0.142	254.31
	0.490	0.400	32.78	0.133	246.14
	0.980	0.388	31.80	0.129	242.42
	1.960	0.385	31.55	0.128	241.48
	2.940	0.382	31.30	0.127	240.53
M2	0.245	0.418	34.26	0.139	286.98
	0.490	0.391	32.04	0.130	277.56
	0.980	0.378	30.98	0.126	272.91
	1.960	0.367	30.08	0.122	268.90
	2.940	0.364	29.83	0.121	267.80
M3	0.245	0.405	33.19	0.135	405.60
	0.490	0.363	29.75	0.121	391.58
	0.980	0.335	27.45	0.111	376.18
	1.960	0.312	25.57	0.104	363.04
	2.940	0.305	24.99	0.101	358.94
M4	0.245	0.318	26.06	0.106	305.80
	0.490	0.267	21.88	0.089	280.21
	0.980	0.248	20.32	0.082	270.05
	1.960	0.246	20.16	0.082	268.96
	2.940	0.238	19.50	0.079	264.55
M5	0.245	0.285	23.35	0.095	309.24
	0.490	0.249	20.40	0.083	289.05
	0.980	0.229	18.76	0.076	277.20
	1.960	0.218	17.86	0.072	270.46
	2.940	0.210	17.21	0.070	265.45

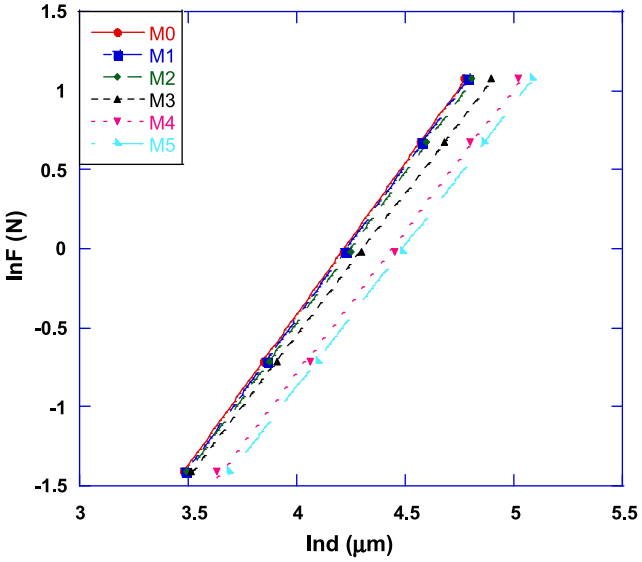

Fig. 5 Variation of applied load $\ln F$ with diagonal $\ln d$ for the samples

tion (EPD) models allow us to examine the corresponding microhardness behaviors belonging to the pure Bi-2212 and Nd-doped Bi-2212 superconducting samples.

3.5.1 Meyer's Law

Meyer's law used to describe the *ISE* behavior is an empirical relationship between indentation load (F) and the indentation size (d) [37]:

$$F = A_1 d^n \tag{4}$$

where A is a constant and the exponent n is known as Meyer index, used to be a measure of the ISE feature. Generally, while $n < 2$ indicates the normal ISE behavior, $n > 2$ indicates RISE behavior in materials [38, 39]. When $n = 2$, it is referred to Kick's Law that can be regarded as a modified Meyer law:

$$F = A_1 d^2 \tag{5}$$

The *InF–Ind* graphs of the pure and Nd-doped Bi-2212 superconductors are given in Fig. 5. One can that n values are smaller than 2 ($n < 2$) for each sample. This is because all the samples obey the ISE behavior as a consequence of the displacement character with the applied test load. In fact, the decrement in the n values guarantees that addition of Nd leads to exhibit more the ISE nature of the samples. Moreover, it is necessary to underline that n values vary between 1 and 1.6 only for the hard materials whereas higher values ($n > 1.6$) are attributed to the soft materials [6]. Based on the results obtained from the samples prepared, each of them is regarded as the soft material (Table 3).

Table 3 Best-fit results of experimental data according to Meyer's law

Samples	Slope n_k	$\ln_{A1k}$ (GPa)
M0	1.91	−8.073
M1	1.91	−8.111
M2	1.89	−8.049
M3	1.79	−7.723
M4	1.80	−8.013
M5	1.79	−8.032

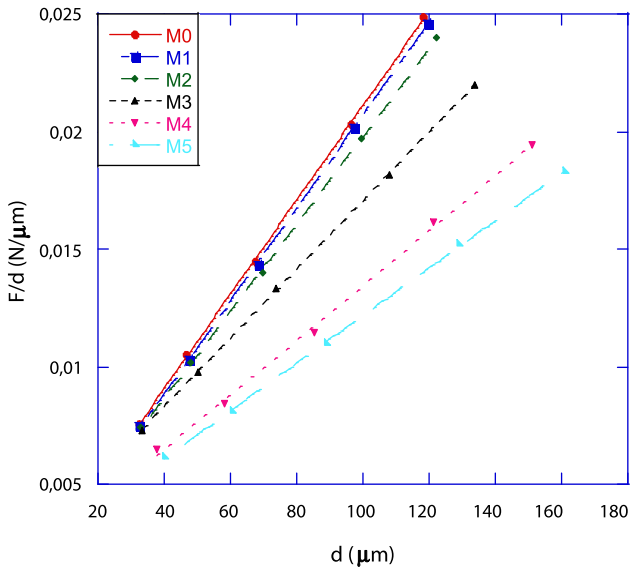

Fig. 6 Plots of F/d versus d for the samples

3.5.2 Analysis of PSR Model

Proportional Specimen Resistance (PSR) model proposed by Li and Bradt can be considered as a modified form of the Hays–Kendall approach. In the current model, the specimen resistance is not constant, so the indentation depth increases linearly:

$$\frac{F}{d} = \alpha + \beta d \tag{6}$$

It is customary to say that Eq. (4) is of a similar form with restoring force ($F = -kx$) of a compressed or extended spring. Consequently, the effective indentation load (F) and indentation size (d) are related as

$$F_{\text{eff}} = F_{\max} - W = F_{\max} - a_1 d = a_2 d^2 \tag{7}$$

where a_1 and a_2 are constants related to the elastic and plastic properties of a material (Fig. 6). Indeed, a_2 is a measure of load-independent microhardness. It can be seen from Table 4 that constant a_1 is positive for all the samples. This result confirms that the plastic deformation as well as the

Table 4 Best-fit results of experimental data according to *PSR* model

Samples	$a_1 \times 10^{-4}$ (N)	$a_2 \times 10^{-5}$ (N/μm)	Load independent hardness H_{PSR} (GPa)	Load dependent hardness H_V (GPa)
M0	10.41	20.06	0.371	0.390–0.392
M1	9.24	19.78	0.355	0.382–0.385
M2	12.02	18.58	0.344	0.364–0.367
M3	24.78	14.58	0.270	0.305–0.312
M4	17.94	11.64	0.216	0.238–0.246
M5	20.47	10.12	0.187	0.210–0.218

Table 5 The calculated load-independent H_0, E_0, Y_0 and K_{IC} for the samples

Samples	H_0 (GPa)	E_0 (GPa)	Y_0 (GPa)	K_{IC} (Pa/m$^{1/2}$)	H_V (GPa)
M0	0.371	30.408	0.123	251.61	0.390–0.392
M1	0.355	29.096	0.118	231.88	0.382–0.385
M2	0.344	28.195	0.114	260.34	0.364–0.367
M3	0.270	22.130	0.090	331.17	0.305–0.312
M4	0.216	17.704	0.072	252.09	0.238–0.246
M5	0.187	15.327	0.062	250.53	0.210–0.218

elastic is produced in the samples presenting the ISE behavior. The load-independent microhardness values calculated in accordance with the PSR model are given in Table 4. It is obvious from the table that the transition values of the samples to the plateau are quite far from the microhardness values calculated using the PSR model [38]. Therefore, it indicates that the PSR model is not adequate for the determination of true microhardness values of both the pure and the Nd-doped Bi-2212 superconducting materials.

Additionally, load-independent elastic modulus, yield strength and fracture toughness values are calculated using load-independent H_{PSR} value and the findings obtained are numerically listed in Table 5. According to the results, sharper decrease in the load-independent E_0, Y_0 and K_{IC} values is observed as compared to load-dependent values. Similar results can be encountered in the literature for other materials [32, 33, 40].

3.5.3 Analysis of MPSR Model

In order to investigate ISE behavior, Gong et al. [41] suggested the modified PSR model:

$$F = W_2 + A_4 d + A_5 d^2 \tag{8}$$

where a_0 is a constant being related to the surface residual stresses associated with the surface machining, and the physical meanings of parameters a_1 and a_2 are the same as the ones in the PSR model. The values of a_0, a_1, a_2 and related load-independent microhardness values are depicted in Table 6. As seen from the table, the values of load-independent microhardness values calculated by MPSR model are far from the values of the plateau region. As a result, the MPSR model is not suitable for the description of the mechanical properties of the prepared materials (Fig. 7).

Table 6 Best-fit results of experimental data according to *MPSR* model

Samples	a_0 (N)	$a_1 \times 10^{-5}$ (N/μm)	$a_2 \times 10^{-5}$ (N/μm^2)	H_{MPSR} (GPa)	H_V (GPa)
M0	0.028	5.60	20.74	0.384	0.390–0.392
M1	0.026	1.67	20.42	0.374	0.382–0.385
M2	0.034	3.64	19.37	0.359	0.364–0.367
M3	0.002	25.65	14.52	0.269	0.305–0.312
M4	0.032	79.49	12.23	0.226	0.238–0.246
M5	0.009	22.86	10.00	0.185	0.210–0.218

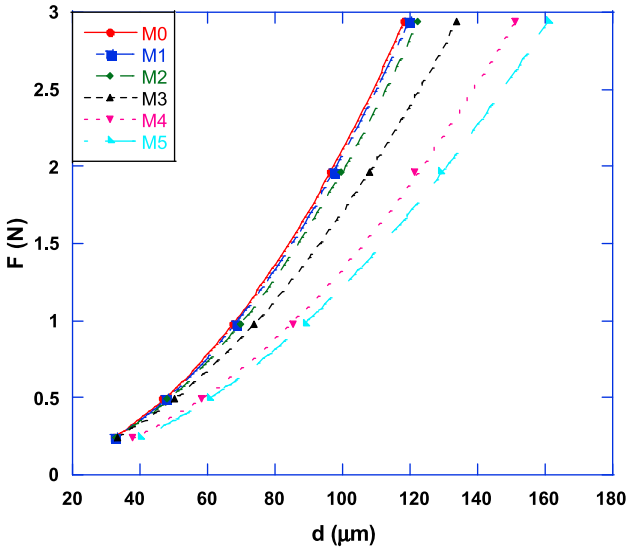

Fig. 7 Variation of applied load with the indentation diagonal length for the samples

3.5.4 Analysis of EPD Model

In indentation tests used, the indentation size is measured after indenter is removed. Hence, the indentation size contracts due to the elastic recovery and Tarkanian et al. (1973) [42] suggested a new term to add to the measured indentation size to find the load-independent microhardness values:

$$F_{max} = A_1 (d_p + d_e)^2 \tag{9}$$

Here, d_e is in correspondence with the correction term which is added to d_p due to elastic recovery when A_1 is an essen-

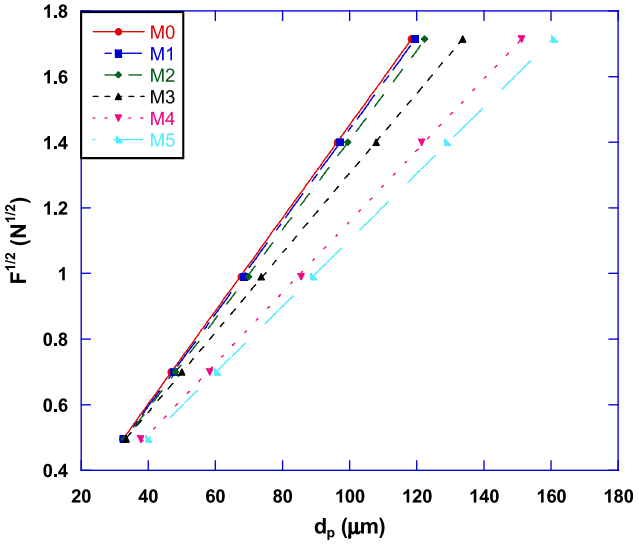

Fig. 8 Plots of diagonal length versus square root of applied loads for the samples

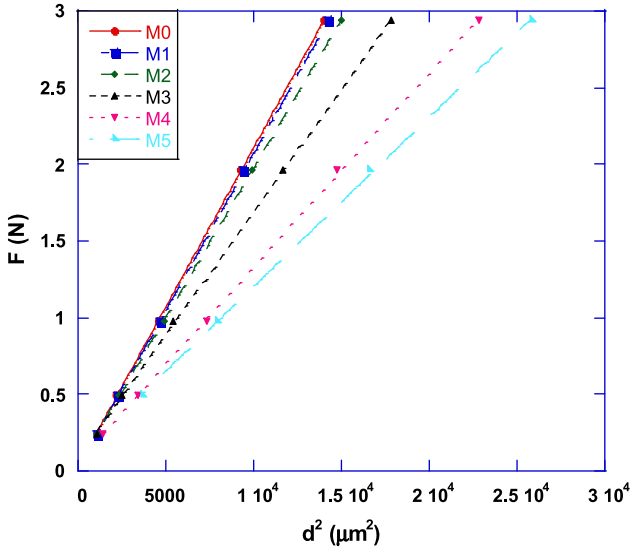

Fig. 9 Graph of the applied load against the square of the diagonal length for the samples

Table 7 Best-fit results of experimental data according to *EPD* model

Samples	A_1 (N/μm^2)	d_e (μm)	H_{EPD} (GPa)	H_V (GPa)
M0	0.0141	0.035	0.368	0.390–0.392
M1	0.0140	0.031	0.363	0.382–0.385
M2	0.0136	0.041	0.342	0.364–0.367
M3	0.0121	0.091	0.271	0.305–0.312
M4	0.0108	0.074	0.217	0.238–0.246
M5	0.0101	0.090	0.189	0.210–0.218

Table 8 Best-fit results of experimental data according to *HK* model

Samples	$C_1 \times 10^{-5}$	W_{HK} (N)	H_{HK} (GPa)	H_V (GPa)
M0	20.78	0.030	0.385	0.390–0.392
M1	20.43	0.026	0.378	0.382–0.385
M2	19.40	0.035	0.359	0.364–0.367
M3	16.02	0.087	0.297	0.305–0.312
M4	12.64	0.064	0.234	0.238–0.246
M5	11.03	0.100	0.204	0.210–0.218

tial parameter used to calculate the microhardness values. The results obtained are given in Fig. 8. The data calculated from the graph can be seen in Table 7. It is apparent from the table that the value of correction term (d_e) is positive for all the samples. It means that the elastic deformation as well as the plastic deformation is observed throughout the applied loads in the samples. As is well known, the elastic recovery is found in the specimen surface after the removal of the indenter. This effect is experimentally observed only for the materials exhibiting *ISE* behavior and it is also consistent with the literature [43]. Conversely, the opposite of this effect is possible and there may appear only the plastic deformation in the materials with negative d_e values [44]. This result is observed in the materials obeying the *RISE* nature [45, 46]. It should be noted here that in these materials the microhardness values increase with increasing the applied indentation test load.

3.5.5 Analysis of the Hays–Kendall Approach

Hays and Kendall suggested that there exists a minimum level (W) of the applied test load to produce an indentation [47, 48]. Here, W is attributed to the resistance of the sample against the load applied. Unless the applied indentation test load exceeds the resistance value, the permanent deformation does not appear in the material but only the elastic deformation does. Thereby, Hays and Kendall proposed that the experimentally measured indentation size is proportional to an effective load as given below (Fig. 9):

$$F_{\mathrm{eff}} = F_{\mathrm{max}} - W = C_1 d^2 \tag{10}$$

where C_1 is a constant related to the applied test load and W the minimum load necessary to initiate the permanent deformation. The load-independent W and C_1 values determined are displayed in Table 8. The positive values of W may be attributed to the fact that the applied load is sufficient to produce the elastic deformation as well as the plastic deformation in the specimen [34, 42]. According to the results observed, both the elastic and plastic deformations are observed in pure and Nd-doped Bi-2212 superconductors.

As a conclusion, the microhardness values calculated using HK approach are quite close to those of the plateau (saturation) region as compared to other model results for all the samples exhibiting the *ISE* behavior. It must be empha-

Table 9 The results of load-dependent Vickers microhardness at the plateau region and load-independent hardness values calculated using *PSR*, *MPSR*, *EPD* and *HK* models

Samples	H_V (plateau region) (GPa)	H_{PSR} (GPa)	H_{MSPR} (GPa)	H_{EPD} (GPa)	H_{HK} (GPa)
M0	0.390–0.392	0.371	0.384	0.368	0.385
M1	0.382–0.385	0.355	0.374	0.363	0.378
M2	0.364–0.367	0.344	0.359	0.342	0.359
M3	0.305–0.312	0.270	0.269	0.271	0.297
M4	0.238–0.246	0.216	0.226	0.217	0.234
M5	0.210–0.218	0.187	0.185	0.189	0.204

sized that the Hays–Kendall approach is the most appropriate model to analyze the mechanical properties of pure and Nd-doped Bi-2212 superconducting ceramics (Table 9). Similar evidences can be observed in the literature [49–51].

4 Conclusion

In the exhaustive study, the role of the Nd inclusion in the superconducting matrix on the structural and mechanical properties of the Bi-2212 ceramics prepared by solid-state reaction method is investigated by means of the standard experimental methods as regards the XRD, SEM and Vickers microhardness measurements and the following results are observed.

- According to the XRD analysis, whereas the c lattice parameter and Bi-2212 phase ratio tend to decrease monotonously, the a parameter and Bi-2201 phase ratio increase systematically with the increase of Nd in the layered structures. These results explain why the grain size values calculated from Scherrer–Warren equation reduce regularly with the doping level.
- Moreover, the SEM micrographs show that the crystal plane alignment (texturing), grain connectivity, crystallinity and layered grain growth systematically decrease with the increase of the Nd impurities in the Bi-2212 superconducting matrix, confirming that the Nd inclusion is unfavorable for the formation of the Bi-2212 superconducting phase.
- Based on the EDS analyses, the Nd additives in the system are effectively introduced into the microstructure of the Bi-2212 superconducting phase by replacing Sr elements.
- Vickers microhardness, elastic modulus, yield strength and fracture toughness values computed are noted to decrease with increasing the applied test load and Nd doping. The fundamental reason of the decrement is the ISE behavior of the materials. Besides, the ISE nature of the samples improves with the increase of the Nd impurities.
- The load-independent microhardness (H_0), elastic modulus (E_0), yield strength (Y_0) and fracture toughness (K_{IC}) are calculated for the doped and undoped superconducting samples and these parameters are found to be smaller than the computed load-dependent values (H_V, E, Y and K_{IC}).
- The results of the microhardness measurements are analyzed employing the Meyer's law, PSR, MPSR, EDP models and the Hays–Kendall approach. Based on the findings, the Hays–Kendall approach is found to be the best model describing the microhardness characteristics of the pure and Nd-doped Bi-2212 superconducting samples.

References

1. Onaran, K.: Materials Science Textbook. Science and Technology Publishing, New York (1993)
2. Armstrong, R.W., Ferrantı Louıs, J.R., Thadhanı Naresh, N.: Int. J. Refract. Met. Hard Mater. **24**, 11–16 (2006)
3. Gong, J., Wu, J., Guan, Z.: J. Eur. Ceram. Soc. **19**(15), 2626–2631 (1999)
4. Gong, J., Zhao, Z., Guan, Z., Miao, H.: J. Eur. Ceram. Soc. **20**, 1895–1900 (2000)
5. Gong, J., Miao, H., Zhao, Z., Guan, Z.: Mater. Sci. Eng. A, Struct. Mater.: Prop. Microstruct. Process. **303**, 179–186 (2001)
6. Sahin, O., Uzun, O., Kolemen, U., Duzgun, B., Ucar, N.: Chin. Phys. Lett. **22**, 3137–3140 (2005)
7. Uzun, O., Karaaslan, T., Gogebakan, M., Keskin, M.: J. Alloys Compd. **376**, 149–157 (2004)
8. Uzun, O., Kolemen, U., Celebi, S., Guclu, N.: J. Eur. Ceram. Soc. **25**, 969–977 (2005)
9. Tate, D.R.: Trans. Am. Soc. Mater. **35**, 374–375 (1945)
10. Mott, B.W.: Microindentation Hardness Testing, pp. 101–139. Butterworths, London (1956)
11. Bückle, H.: In: Westbrook, J.H., Conrad, H. (eds.) The Science of Hardness: Testing and Its Research Applications, p. 199. ASME, Metal Park (1973)
12. Upit, G.P., Varchenya, S.A.: In: Westbrook, J.H., Conrad, H. (eds.) The Science of Hardness: Testing and Its Research Applications, pp. 135–144. ASME, Metal Park (1973)
13. Bull, S.J., Page, T.F., Yoffe, E.H.: Philos. Mag. Lett. **59**, 281–288 (1989)
14. Li, H., Bradt, R.C.: J. Mater. Sci. **28**, 917–926 (1993)
15. Li, H., Han, Y.H., Bradt, R.C.: J. Mater. Sci. **29**, 5641–5645 (1994)
16. Liu, Y., Ngan, A.H.W.: Scr. Mater. **44**, 237–241 (2001)
17. Ozturk, O., Yildirim, G., Asikuzun, E., Coskunyurek, M., Yilmazlar, M., Kilic, A.: J. Mater. Sci., Mater. Electron. (2013). doi:10.1007/s10854-013-1456-z
18. Dogruer, M., Karaboga, F., Yildirim, G., Terzioglu, C.: J. Mater. Sci., Mater. Electron. **24**, 2327–2338 (2013)
19. Nguyen-van-huong, C., Hinnen, C., Siffre, J.M.: J. Mater. Sci. **32**, 1725–1731 (1997)
20. Vinu, S., Sarun, P.M., Shabna, R., Biju, A., Syamaprasad, U.: Mater. Lett. **62**, 4421–4424 (2008)
21. Vinu, S., Sarun, P.M., Biju, A., Shabna, R., Guruswamy, P., Syamaprasad, U.: Supercond. Sci. Technol. **21**, 045001 (2008)
22. Yildirim, G., Bal, S., Varilci, A.: J. Supercond. Nov. Magn. **25**, 1655–1663 (2012)
23. Yildirim, G., Dogruer, M., Karaboga, F., Terzioglu, C.: J. Alloys Compd. **584**, 344–351 (2014)
24. Moodera, J.S., Meservey, R., Tkaczyk, J.E., Hao, C.X., Gibson, G.A., Tedrow, P.M.: Phys. Rev. B **37**, 619 (1988)

25. Ozturk, O., Asikuzun, E., Yildirim, G.: J. Mater. Sci., Mater. Electron. **24**, 1274–1281 (2013)
26. Yildirim, G.: J. Alloys Compd. **578**, 526–535 (2013)
27. Guner, S.B., Gorur, O., Celik, S., Dogruer, M., Yildirim, G., Varilci, A., Terzioglu, C.: J. Alloys Compd. **540**, 260–266 (2012)
28. Biju, A., Syamaprasad, U., Rao, A., Xu, J.G., Sivakumar, K.M., Kuo, Y.K.: Physica C **466**, 69 (2007)
29. Yildirim, G., Bal, S., Yucel, E., Dogruer, M., Akdogan, M., Varilci, A., Terzioglu, C.: J. Supercond. Nov. Magn. **25**, 381–390 (2012)
30. Biju, A., Sarun, P.M., Aloysius, R.P., Syamaprasad, U.: J. Alloys Compd. **454**, 46–51 (2008)
31. Dogruer, M., Karaboga, F., Yildirim, G., Terzioglu, C., Ozturk, O.: J. Mater. Sci., Mater. Electron. **24**, 2659–2666 (2012)
32. Arda, L., Ozturk, O., Asikuzun, E., Ataoglu, S.: Powder Technol. **235**, 479–484 (2013)
33. Celik, S., Ozturk, O., Coskun, E., Asikuzun, E., Ozturk, K., Sarihan, M., Terzioglu, C.: J. Mater. Sci., Mater. Electron. (2013). doi:10.1007/s10854-013-1082-9
34. Awad, R., Abou-Aly, A.I., Kamal, M., Anas, M.: J. Supercond. Nov. Magn. **24**, 1947–1956 (2011)
35. Sangwal, K.: Mater. Chem. Phys. **63**, 145–152 (2000)
36. Zalaoglu, Y., Bekiroglu, E., Dogruer, M., Yildirim, G., Ozturk, O., Terzioglu, C.: J. Mater. Sci., Mater. Electron. **24**, 2339–2345 (2013)
37. Tabor, D.: The hardness of metals. Philos. Mag., A **74**, 1207 (1996)
38. Quinn, J.B., Quinn, G.D.: J. Mater. Sci. **32**, 4331–4346 (1997)
39. Asikuzun, E., Ozturk, O., Cetinkara, H.A., Yildirim, G., Varilci, A., Yilmazlar, M., Terzioglu, C.: J. Mater. Sci., Mater. Electron. **23**, 1001–1010 (2012)
40. Cavdar, S., Deniz, E., Koralay, H., Ozturk, O., Erdem, M., Gunen, A.: J. Supercond. Nov. Magn. **25**, 2297–2307 (2012)
41. Turkoz, M.B., Nezir, S., Ozturk, O., Asikuzun, E., Yildirim, G., Terzioglu, C., Varilci, A.: J. Mater. Sci., Mater. Electron. **24**, 2414–2421 (2013)
42. Tarkanian, M.L., Neumann, J.P., Raymond, L.: Determination of the Temperature Dependence of 100 and 112 Slip in Tungsten from Knoop Hardness Measurements, pp. 187–198. ASME, Metal Park, (1973)
43. Ma, Q., Clarke, D.R.: J. Mater. Res. **10**, 853–863 (1995)
44. Fröhlich, F., Grau, P., Grellmann, W.: Phys. Status Solidi A **42**, 79–89 (1977)
45. Oliver, W.C., Hutchings, R., Pethica, J.B.: Measurement of hardness at indentation depths as small as 20 nm. In: Blau, P.J., Lawn, B.R. (eds.) Microindentation Techniques in Materials Science and Engineering, pp. 90–108. ASTM, Philadelpia (1986)
46. Michels, B.D., Frischat, G.H.: J. Mater. Sci. **17**, 329–334 (1982)
47. Yilmazlar, M., Ozturk, O., Gorur, O., Belenli, I., Terzioglu, C.: Supercond. Sci. Technol. **20**, 365–371 (2007)
48. Dogruer, M., Yildirim, G., Ozturk, O., Varilci, A., Soylu, N., Gorur, O., Terzioglu, C.: J. Mater. Sci., Mater. Electron. **24**, 1264–1273 (2013)
49. Hays, C., Kendall, E.G.: Metallurgica **6**, 275–282 (1973)
50. Upit, G.P., Varchenya, S.A.: Phys. Status Solidi B **17**, 831–835 (1966)
51. Koralay, H., Arslan, A., Cavdar, S., Ozturk, O., Asikuzun, E., Gunen, A., Tasci, A.T.: J. Mater. Sci., Mater. Electron. (2013). doi:10.1007/s10854-013-1396-7